Available online at www.sciencedirect.com
SCIENCE DIRECT®
Polymer 45 (2004) 2729–2736
polymer
www.elsevier.com/locate/polymer

Abrasive wear micromechanisms of oriented polymers

J. Cayer-Barrioz[a,*], D. Mazuyer[a], Ph. Kapsa[a], A. Chateauminois[b], G. Robert[c]

[a]*Laboratoire de Tribologie et de Dynamique des Systèmes, UMR 5513, Ecole Centrale de Lyon, 36 avenue Guy de Collongue, 69130 Ecully, France*
[b]*Laboratoire de Physico-Chimie Structurale et Macromoléculaire, UMR 7615, ESPCI, 10 rue Vauquelin, 75231 Paris, France*
[c]*Rhodia Centre de Recherches de Lyon, 85 avenue des frères Perret, 69192 Saint-Fons, France*

Received 17 November 2003; received in revised form 5 February 2004; accepted 11 February 2004

Abstract

For successful use in textile applications, synthetic fibres must have an excellent wear resistance. This paper analyses the wear micromechanisms of polymeric fibres as a function of microstructural parameters such as molecular orientation and degree of crystallinity. A series of poly(amide) 6 fibres differing in their molecular weight has been studied under abrasive wear conditions. From an examination of the wear kinetics, it was concluded that the nature of wear macromechanisms is independent of the experimental conditions and fibre molecular weight. By means of wide angle X-ray scattering, it was shown that the level of molecular orientation within the amorphous phase was correlated to the wear damage resistance. From these observations, an interpretation of the wear micromechanisms is proposed. It relies upon the localised cavitation of microvoids within the interfibrillar amorphous domains of the microfibrillar structure under the abrasive action of the sliding micro-asperities. The coalescence of these microvoids activates relative displacements between microfibrils, which eventually leads to the splitting of clusters of microfibrils and wear losses. A combination of this material loss with creep results in fibre failure. The observed micromechanism emphasises the role of the molecular orientation on wear resistance.

Keywords: Abrasive wear; Microstructure; Molecular weight

1. Introduction

The wear behaviour of polymeric materials has drawn a considerable interest over the past years. Although a wide variety of isotropic and bulk polymeric materials have been investigated under different wear conditions [1–4], less attention was paid to the frictional damage of highly anisotropic polymers such as synthetic fibres [5]. The wear resistance of various fibres such as poly(amide)s fibres is, however, relevant in many applications from textiles to car tyres, where it is particularly desirable to obtain some insight into the effects of molecular orientation and structure on the fibres tribological properties.

The most common process for producing synthetic fibres is melt spinning followed by an additional hot drawing step in order to achieve the required molecular orientation [6]. The development of such an orientation often results in a specific microfibrillar structure. In the context of poly (amide) fibres, Prevorsek et al. [7] have proposed the so-called 'swiss-cheese ' model which applies to the poly (amide) 6 (PA6) fibres investigated in this study. In this description, microfibrils which consist in recurrent series of crystallites and amorphous domains are embedded in an oriented amorphous matrix.

The aim of this paper is to contribute to the understanding of the interrelationships between the microstructure of PA6 fibres and wear damage micromechanisms under abrasive wear conditions. The influence of the molecular weight, which is strongly correlated to molecular orientation, has been especially investigated.

In order to test the wear resistance of small diameter (40×10^{-6} m) PA6 fibres, a specific tribometer has been designed which realises a contact between a single fibre and a rotating abrasive rod. This tribometer is based on the capstan apparatus principle, formerly used by Roselman and Tabor [8] to investigate the friction and wear of carbon fibres. In addition to volumetric wear loss measurements, a detailed insight into the wear micromechanisms as a function of fibre microstructure was provided by scanning electron microscopy (SEM) observations and wide angle

* Corresponding author. Tel.: +33-4-72-18-62-88; fax: +33-4-78-43-33-83.
E-mail address: juliette.cayer-barrioz@ec-lyon.fr (J. Cayer-Barrioz).

0032-3861/$ - see front matter © 2004 Elsevier Ltd. All rights reserved.
doi:10.1016/j.polymer.2004.02.013

X-ray scattering (WAXS). The fibre microstructure and its resulting mechanical properties are known to be highly sensitive to water plasticization effects [9–11]. In order to avoid the effects of a variable moisture environment, the wear properties of the poly(amide) fibres were systematically tested in water immersion.

2. Experimental details

2.1. Materials

The polymers used in this work are PA6 fibres purchased by Rhodia (St Fons, France). Specimens differing in their molecular weight (M_n between 19 and 26 kg/mol) have been elaborated by melt spinning using a twofold drawing ratio. Before starting the tribological measurements, the samples (Table 1) were characterized with respect to their molecular weight M_n, their diameters and their mechanical properties (Young's modulus, E, true failure stress, σ_R, and failure strain, ε_R). The molecular weights have been determined by size exclusion chromatography in dichloromethane. The diameter and tensile properties are measured using a Textechno Statimat tester at 4×10^{-3} m/s, i.e. at 2×10^{-2} s^{-1} for a 0.25 m long specimen, 300 K and 50% relative humidity. For a selected number of fibres in this study, the degree of orientation of the amorphous phase f_a and the relative fraction of oriented amorphous component F_a have been quantified as described in Ref. [12], by means of WAXS performed using the monochromated Cu K_α radiation at 1.54×10^{-10} m on a rotating anode (Fig. 1). The intensity of amorphous peaks can be divided into two components (the isotropic component below the baseline and the anisotropic component above the baseline). Whereas the degree of orientation of the entire amorphous phase f_a is evaluated using the intensity of the total amorphous scattering, F_a (or the fraction of the molecules in the amorphous regions that are preferentially oriented) is

Table 1
Diameter, ϕ, Young's modulus, E, true rupture stress, σ_R, and rupture strain, ε_R, (at 4×10^{-3} m/s, i.e. 2×10^{-2} s^{-1}, 300 K and a relative humidity of 50%), orientation degree, f_a, of the amorphous phase and relative fraction of the oriented amorphous phase, F_a, of PA6 fibres differing in their molecular weight, M_n

Fibre	M_n (kg/mol)	ϕ (10^{-6} m)	E (10^9 Pa)	σ_R (10^6 Pa)	ε_R (%)	f_a	F_a (%)
A	19.00	42		796	60.4	0.366	37.8
B	19.37	35	2.08	694	57.3	0.267	35.5
C	19.90	35	1.80	681	63.8		
D	20.56	33	2.06	676	58.1		
E	21.37	34	1.93	720	63.2	0.211	29.7
F	22.97	35	1.69	658	62.8		
G	23.20	40	1.36	491	60.9	0.164	25.9
H	26.00	42	1.06	492	40.9	0.301	34.6

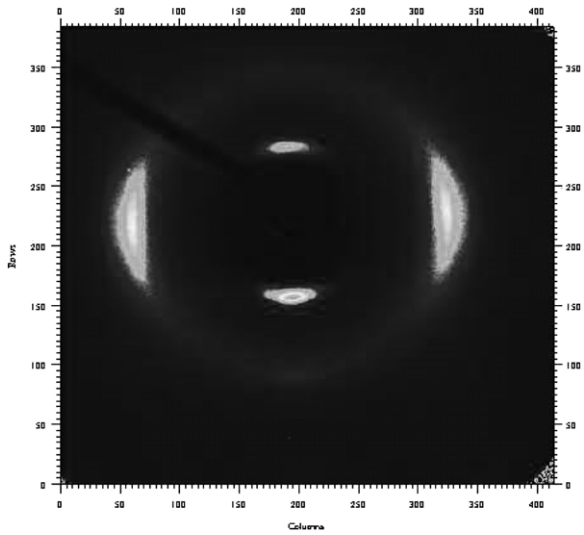

Fig. 1. WAXS pattern obtained with fibre H using a monochromated Cu K_α radiation on a rotating anode. See text for details regarding the obtention method of the amorphous phase characteristics.

calculated as follows:

$$F_a = \frac{A_p}{A_p + A_b} \quad (1)$$

where A_p is the area of the amorphous peak above the baseline and A_b is the intensity below the baseline, $(A_p + A_b)$ being the total scattered intensity from the amorphous phase.

2.2. Abrasive wear tests and experimental procedure

The detailed investigation of the wear mechanisms of polymeric fibres requires an experimental set-up where the roughness of the abrasive counterface, the environment and the sliding velocity can be accurately monitored. For that purpose, a casten machine was designed which realises a contact between a fixed tight fibre and a rotating 'abrasive ' rod immersed in a constant temperature bath of mineral water (Fig. 2). In each experiment, 15 fibres can be simultaneously tested in order to make a statistical analysis of the fibre rupture. A tension F_1 is applied on the free extremity of the fibre by means of a dead weight (between 2×10^{-3} and 7×10^{-3} kg) and pulley system. The force generated by the rod friction is measured on the other end of the fibre by a force transducer. The elongation of one fibre out of 15 is recorded during the experiment via a displacement sensor. The 10^{-2} m diameter abrasive rod is made of steel covered by a hard ceramic coating. The roughness R_a of the rod is 1.6×10^{-6} m and the conical shape asperities present a slope angle of 40°. Fibres are immersed in mineral water 24 h before testing. A detailed description of the experimental set-up can be found in Ref. [13].

Rubenstein had suggested that the plasticization of the polymer takes place with two opposing tribological effects, a decrease in the interface shear strength and an increase in

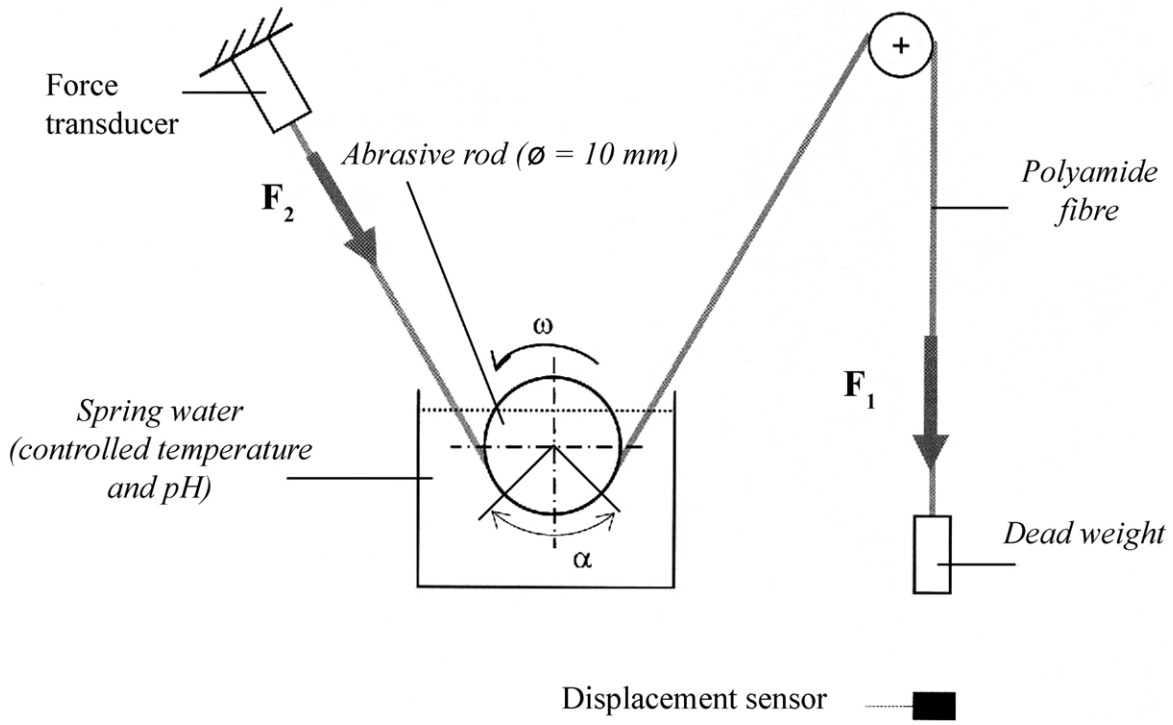

Fig. 2. Schematic description of the tribometer. A fixed tight fibre loaded via a dead weight is rubbed against a rotating abrasive rod. The contact between the fibre and the rod is fully immersed in spring water. The tension, F_2, generated by friction, is recorded by a load transducer, the fibre elongation is measured using a displacement sensor located beneath the dead weight.

the area over which contact is made when the polymer is slid over another surface. He suggested that the increase in the contact area is the more significant effect so that the aqueous lubrication character is rather poor [10,11]. This latter effect has been confirmed within the considered contact as detailed in Ref. [13].

A macroscopic wear criterion was defined as the rod sliding distance leading to the fibre failure, D_R. This wear criterion was found to be independent of the sliding velocity within the investigated speed range, i.e. 0.15–1.6 m/s. A simple thermal analysis of the contact also demonstrated that the cooling capability of the water prevented the fibres from any significant friction induced heating [13].

3. Results

3.1. Fibre wear processes

A macroscopic analysis of the contact deformation modes has been realized, thanks to SEM and AFM observations of the damaged fibres. In the 8×10^{-3} m long contact zone, the same abrasive scratches aligned along the sliding direction are observed on every fibre (Fig. 3(a)). AFM imaging is used to characterize the worn fibres locally and to determine the scratch size (Fig. 3(b)). This size is related to the asperity shape since the abrasive scratches are about 3×10^{-6} m wide and 0.5×10^{-6} m deep. These scratches confirm an abrasive wear mechanism of the fibre and reveal the plastic deformation at the fibre surface. Abrasion causes a progressive diminution of the fibre cross-section from the centre of the contact zone until the failure point. In the neighbourhood of the failure point, the fibre is completely flattened. Fibrillations of a few micrometers thick are also observed along the fibre edges (Fig. 4). These observations are independent of the molecular weight and of the experimental conditions.

3.2. Volumetric wear loss kinetics

Wear tests have been performed on the fibres A and H using various combinations of applied tensile loads (between 3×10^{-3} and 5×10^{-3} kg) and sliding speeds (from 0.15 to 1 m/s). These tests have been interrupted after different sliding distances in order to determine the wear loss kinetics. Using a procedure described elsewhere [13], the volumetric wear losses have been measured from SEM observations of the worn sections of the fibres. Fig. 5 presents the evolution of the estimated wear volume as a function of the sliding distance, D normalized with respect to the sliding distance to fibre failure, D_R. In order to take into account the slight differences between the cross-sections of the various specimens, all the measured wear volumes were normalized with respect to an initial volume defined as the product of the initial fibre cross-section by the theoretical length of contact between the rod and the fibre.

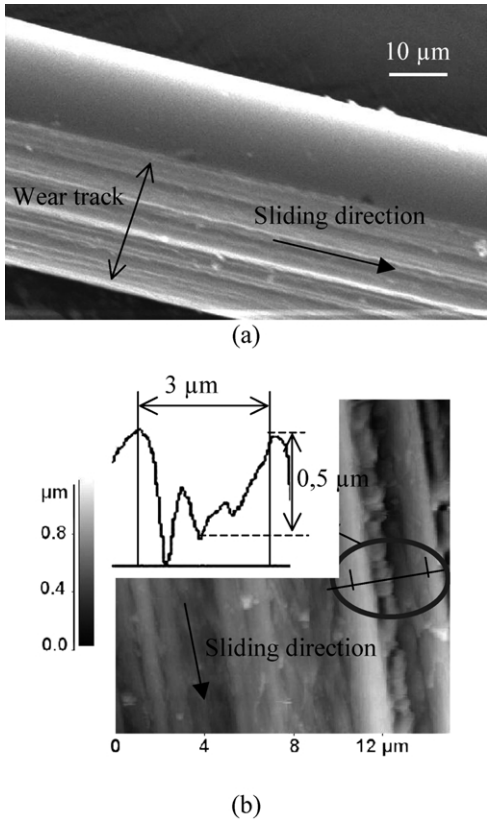

Fig. 3. (a) SEM, and (b) AFM observations of the worn fibres H in the contact zone before the occurrence of rupture (for a 47 m sliding distance). Insert: AFM profile of the worn fibre surface perpendicular to the sliding direction. These observations show abrasive scratches oriented along the sliding direction and extensive surface plastic deformation.

Fig. 5 shows that these normalized wear volumes increase linearly with the wear criterion D/D_R, independently of the loading conditions and of the polymer molecular weight. This observation tends to demonstrate that the nature of the wear damage mechanisms remains essentially unaffected by contact conditions and molecular parameters. From this similarity in the fibre wear mechanisms, the wear kinetics of

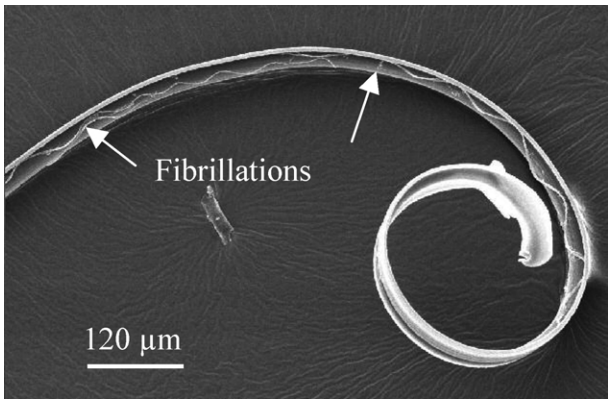

Fig. 4. SEM observations of a worn fibre H after failure. The fibre cross-section decreases progressively along the contact zone until it flattens close to the failure point. A few micrometer thick defibrillations are observed along the fibre edges.

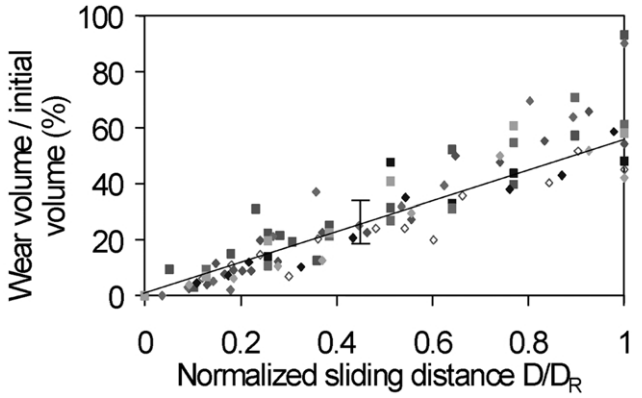

Fig. 5. Changes in the wear volume as a function of the normalized sliding distance, D/D_R, for fibres A and H under different tensile loads (3×10^{-3} and 5×10^{-3} kg) and sliding velocities (from 0.15 to 1 m/s). (■) Fibre A, (◆) Fibre H. The slow (respectively, fast) velocity corresponds to the dark (respectively, pale) symbols. The hollow symbols correspond to the tests carried out at 5×10^{-3} kg. D_R denotes the sliding distance to fibre failure.

any PA6 fibre can be predicted from the knowledge of its initial cross-section and its respective wear criterion, D_R. An empirical wear law has been established, which correlates the measured wear volume, V_{wear}, to the applied load, F_1, the sliding distance, D, and the molecular weight, M_n, of the fibres:

$$V_{wear} \propto \frac{F_1^2 D}{M_n} \tag{2}$$

This wear law reveals the strong sensitivity of the fibre abrasion resistance to the molecular weight: the higher the molecular weight, the lower the wear volume, the better the wear resistance.

3.3. Analysis of the interactions between wear losses and creep behaviour

The wear damage analysis detailed above shows that the final fibre failure results from the combined action of the applied tensile load and the material losses associated to abrasion. The latter process results in a progressive decrease in the actual fibre cross-section throughout the wear test, which in turn induces a continuous increase in the true tensile stress applied to the worn portion of the fibre. Although the unworn fibres were found to be nearly insensitive to creep within the investigated range of applied tensile loads, it may be envisaged that some threshold for non-linear creep is achieved as a result of wear losses. A rather unusual situation can thus be encountered where the surface degradation and the mechanical response of the bulk material are strongly intricate. In order to investigate such effects, an attempt is made to estimate the true strains and stresses experienced by the worn portions of the fibres during the course of an abrasion test.

The determination of the wear kinetic gives the evolution of the fibre cross-section throughout the wear test. From the

former values and the friction generated load F_2, true stresses in the fibre can be calculated as a function of time. A preliminary study concerning the origin of the fibre elongation has revealed that only the portion of the fibre which is localised in the contact (i.e. 8×10^{-3} m) is lengthened during a wear experiment. Therefore, true strains in the contact zone have been evaluated as a function of time from the elongation measurements carried out during the wear test.

In addition, static creep experiments under a purely tensile loading have been carried out for various applied loads (which correspond to true stresses up to 450×10^6 Pa) using the water saturated fibres A and H. The elongation of the fibres has been measured as a function of time until the measured strain reached nearly a constant value within a time corresponding to the mean duration of a wear test (about 600 s). The corresponding values of the 'stabilized' elongation were used to measure a true creep strain under the considered applied tensile load. Fig. 6 compares the 'true stress–true strain curves' obtained for creep and wear experiments on fibre H for a 3×10^{-3} kg weight and a sliding speed of 0.15 m/s. Regarding wear experiments, two stages can clearly be distinguished:

(i) a first stage where material losses resulting from abrasion are the main mechanism (the fibre cross-section diminishes by about 50%). During this stage, the tensile stress applied to the worn section of the fibres remains inferior to the threshold creep stress (about 80×10^6 Pa), which can be defined as the value below which no significant creep strain is measured during a time corresponding to the wear experiments. However, a significant elongation of the fibre is noticed during this first step which cannot be explained by considering only the action of the applied tensile load F_1. This result tends to demonstrate that the shear stresses generated by the sliding of the rod asperities can activate some bulk creep mechanisms within the fibres. Assuming strong interaction between the molecular chain and the asperity surface, it may be suggested that molecular chains are stretched out and sheared when the asperity is sliding at the polymer surface. This stretching and shearing might lead to microfibrils relative motion. This emphasises the role of the interfacial friction.

(ii) During the second stage, a coupling between wear losses, and tensile and compressive stress appears, which is characterized by a strong change in the shape of the fibre cross-section. As the true applied stress exceeds the creep threshold, the fibres are progressively flattened in the form of thin ribbons. The final fibre failure is observed when the applied true stress reaches the creep failure strain (about 600×10^6 Pa).

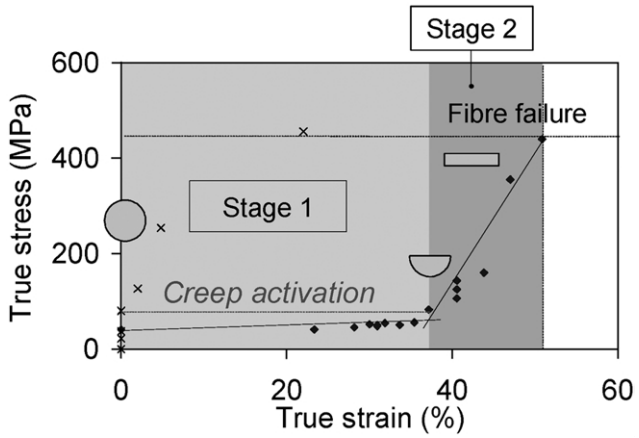

Fig. 6. Identification of two successive wear stages from the change in the fibre true tensile stress as a function of true strain (fibre H, 3×10^{-3} kg, 0.15 m/s). (×) Tensile creep experiments. (True strains refer to the fibre elongation achieved after a time corresponding to the duration of a wear experiment). (◆) true stress and true strain achieved during the course of a wear test. True stress and strain values have been calculated from SEM measurements of the worn fibre cross-section. The schematic shape of the fibre cross-section is also shown. See text for details regarding stage 1 and stage 2.

Fig. 7 presents the true stress–true strain curves obtained for wear experiments on fibre A ($M_n = 19$ kg/mol) and H ($M_n = 26$ kg/mol) for a 3×10^{-3} kg dead weight and a sliding speed varying from 0.05 to 1 m/s. The two wear stages, previously defined, were also observed independently of the nature of the fibres and of the experimental conditions. However, the transition to wear activated creep mechanisms appears to be sensitive to the molecular weight. This might be explained by the influence of the molecular weight on fibre creep [14]. It is therefore clear that in all cases the wear process promotes a continuous diminution of the fibre cross-section until the creep failure stress is locally reached.

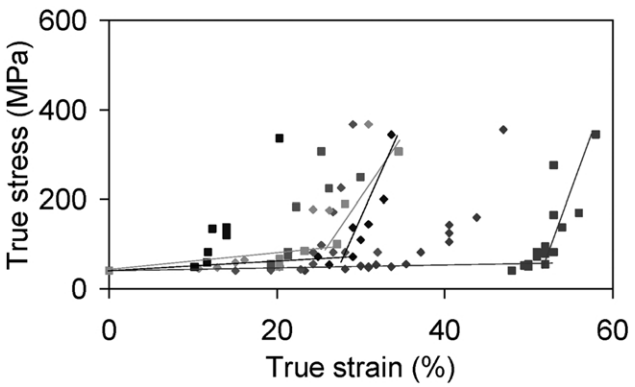

Fig. 7. Change in the fibre true tensile stress as a function of true strain for fibres A and H during wear tests. ■ Fibre A, ◆ Fibre H. The slow (respectively, fast) velocity is represented by dark (respectively, pale) symbols as explained in Fig. 5. The change of slope is attributed to the modification of stage.

3.4. Correlation between fibre microstructure and wear processes

The contribution of the fibre microstructure to wear damage micromechanisms has been considered using fibres with different molecular weights (fibres A–H in Table 1). As detailed in Table 1, this procedure allows to vary the mechanical properties (modulus, failure stress and strain) and microstructural parameters such as the level of orientation of the amorphous phase and the degree of crystallinity. A preliminary study shows that the ratio D_R over the initial cross-section is constant for a given material. As a consequence, the wear resistance of the various fibres is compared by means of the criterion, $D_R^* = D_R$/initial cross-section. All the related wear tests were carried out at a 300 rpm speed (i.e. 0.15 m/s) and under a 3×10^{-3} kg dead weight. In Fig. 8, fibres mechanical properties such as true failure stress and Young's modulus are plotted as a function of D_R^*. It is noted that an increase in failure stress or Young's modulus is associated with a decrease in the fibre wear resistance. This effect could be due to a higher number of extended tie-molecules (since an increase in PA6 fibres Young's modulus is attributed to an augmentation of the volume fraction of the extended-chain molecules in the amorphous phase [15]), which could be an indication of the influence of the amorphous phase on the fibre tribological behaviour.

A further indication of the contribution of the amorphous phase to wear damage can be found in Fig. 9 where the wear resistance has been represented as a function of both the orientation degree, f_a, of the amorphous phase and the relative fraction of oriented component, F_a, as determined by WAXS (Table 1). It can be concluded from this figure that a strongly oriented amorphous phase (probably located in the interfibrillar domains) and an important quantity of it decrease the fibre wear resistance.

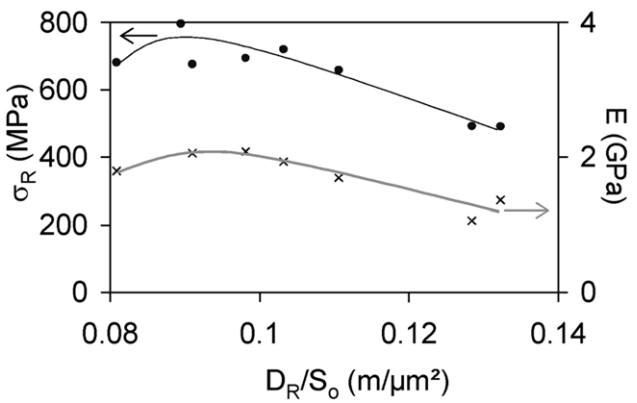

Fig. 8. Correlation between the wear resistance (as quantified by the ratio of the sliding distance to fibre failure, D_R, to the initial fibre cross-section, S_o) and the fibre mechanical properties. ● True failure stress, × Young's modulus. The wear tests were performed at 0.15 m/s under 3×10^{-3} kg.

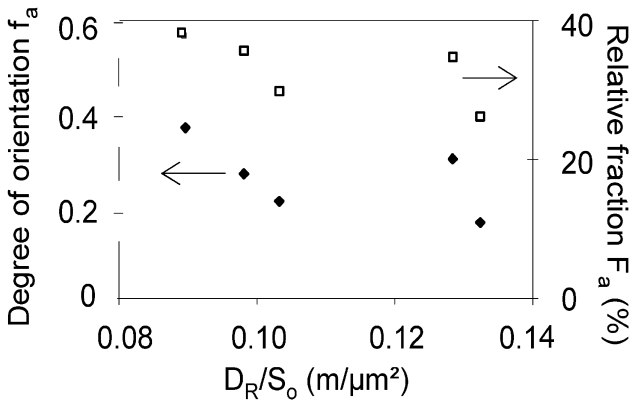

Fig. 9. Influence of the degree of orientation of the amorphous phase, f_a (◆), and of the relative fraction of oriented component, F_a (□), on the wear resistance. Wear tests were carried out at 0.15 m/s and 3×10^{-3} kg. f_a and F_a were quantified as described in Ref. [12].

4. Discussion

4.1. Wear micromechanisms

From SEM observations, it appears that wear damage is to some extent associated to the nucleation and growth of cavities within the polyamide fibres (but no evidence of crazing processes was detected from the SEM observations of the worn fibre surfaces). Such cavitation phenomena have been reported by Plummer et al. [16] and Gensler et al. [17] in various semi-crystalline polymers such as polyethylene or polypropylene during creep, cyclic fatigue or tensile tests in a range of velocity up to 1 m/s. Accordingly, a tentative description of wear micromechanisms can be proposed which relies on the nucleation and growth of internal cavities under the ploughing action of the sliding micro-asperities. Because of the fibrillar structure of the studied material, it can be assumed that these voids are mainly localised in the interfibrillar amorphous domains (Fig. 10). The void nucleation might be attributed to the existence of tensile stresses in the rear portion of the contact, which may induce negative hydrostatic pressure. Tensile stress generated during the wear process promotes the stretching of the microvoids parallel to the fibre axis. These cavitation defects may coalesce and lead to the formation of splitting clusters of microfibrils as observed Fig. 11.

The propagation of the fracture is then due to the formation and growth of cavitation microvoids.

4.2. Orientation of the amorphous phase

The study of the interrelationships between wear and microstructure structure (as affected by changing the molecular weight) has revealed the influence of the oriented amorphous phase on the fibre wear resistance, which is explained by the considering wear micromechanisms based

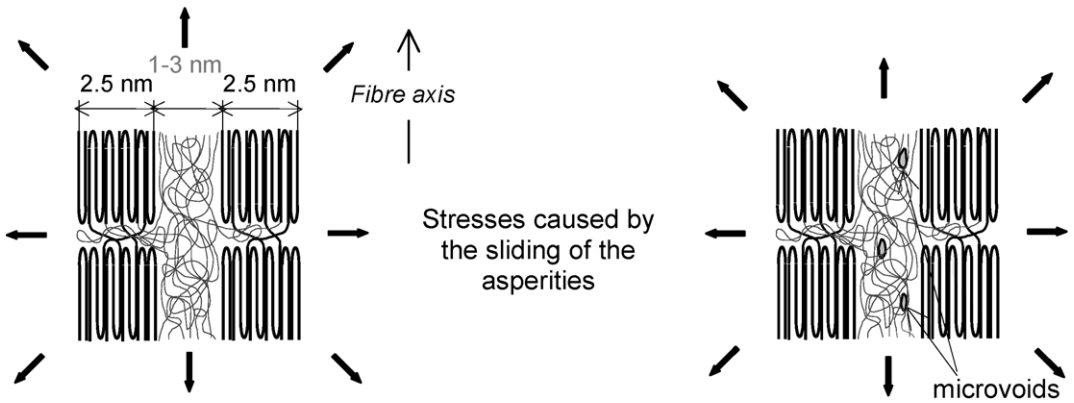

Fig. 10. Schematic description of the cavitation processes occurring within the interfibrillar amorphous phase of the PA6 fibres: (a) stretching of the polymer, (b) microvoids formation.

on the nucleation and coalescence of internal cavities within the fibres. Fig. 12 depicts schematically that the more the amorphous phase is oriented and the higher is the quantity of the anisotropic amorphous component, the easier the microvoids coalesce and the faster is the wear kinetic.

It is also noteworthy that microvoids propagation probably activates the relative sliding between microfibrils since the number of entanglements between microfibrils is assumed to decrease as the microvoids coalesce. Therefore, relation (2) describing the wear acceleration with a decreasing molecular weight can be explained by the dependence between the molecular weight and the microvoids propagation.

5. Conclusions

This study focused on the wear mechanisms of single PA6 fibres under abrasive wear conditions. SEM observations and wear volume analyses show that similar damage micromechanisms are involved in the wear response of fibres of variable diameters and molecular weights under a wide range of experimental conditions. Accordingly, the changes in the wear volumes as a function of the sliding distance are described using a single empirical wear law which incorporates the fibre molecular weight as one of the main material parameters.

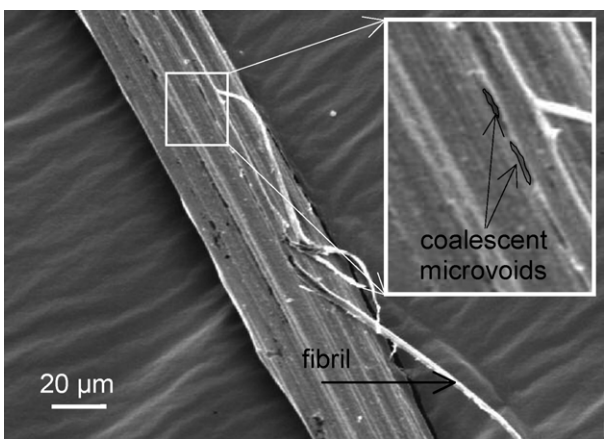

Fig. 11. SEM observations of the coalescence of microvoids and of the associated splitting of fibrils. Wear experiments have been performed at 2000 rpm, i.e. 1 m/s and a 3×10^{-3} kg dead weight and interrupted for a sliding distance of 126 m.

A detailed investigation of creep and wear mechanisms allows to define two successive wear stages: a first stage where material losses resulting from abrasion are the dominant process and a second stage which involves complex interactions between material losses and creep processes induced under the combined action of tensile, shear and compressive stresses. Wear activated creep eventually results in the fibre failure.

A tentative description has been made in order to interpret the effects of the molecular weight on the wear behaviour of PA6 fibres. The model assumes that the sliding micro-asperities induce the formation of microvoids in the interfibrillar amorphous domains by a cavitation process. These microvoids can coalesce and subsequently lead to the splitting of clusters of microfibrils and to the removal of wear debris. Relative displacements between microfibrils could be activated by microvoid formation and by the decrease in the fibre cross-section (which entails a rise of the local stress and then the fibre failure). Such cavitation processes present two specificities:

(i) their origin can be attributed to the interfacial friction,
(ii) the localisation and the propagation of the microvoids are correlated to the microfibrillar structure, i.e. to the macromolecular orientation.

In this description of the wear micromechanisms, the dependence of the wear resistance on the molecular weight is essentially attributed to changes in the orientation of the amorphous phase which are observed using WAXS.

The present work is nevertheless based on hypotheses, especially concerning the role of the interfacial friction. It would be interesting to look at the microstructural

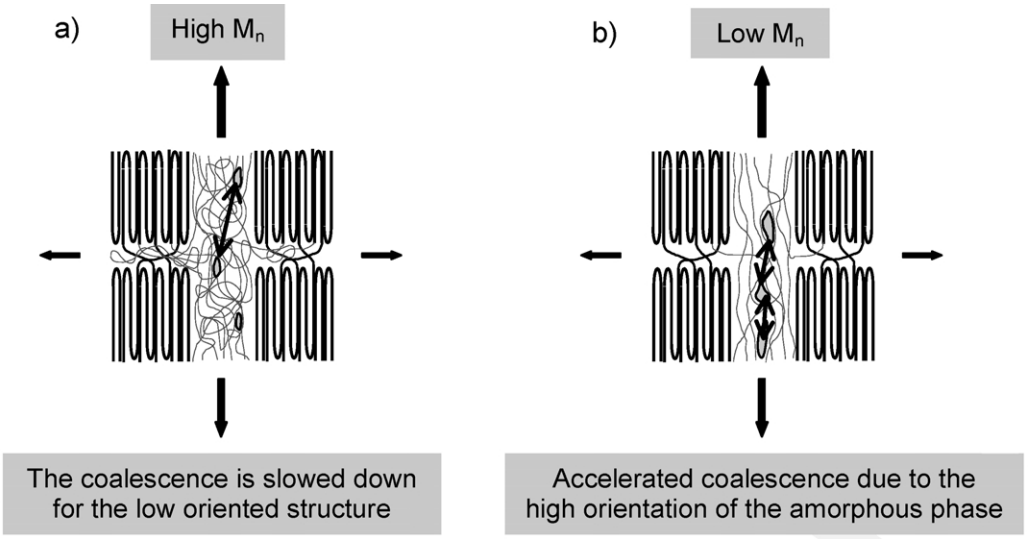

Fig. 12. Influence of the amorphous phase orientation on the propagation of microvoids: (a) low orientation (b) high orientation.

modifications induced by friction and wear by means of WAXS analysis of damaged fibres. Moreover, the correlation between the fibre manufacturing process and the resulting fibrillar structure clearly needs to be studied more in details. Nevertheless, the identification of relevant wear micro-mechanisms and of their interdependence with macromolecular orientation represents a first step in the understanding of the wear of poly(amide) fibre materials.

Acknowledgements

Rhodia Technical Fibres is acknowledged for its financial support for this work. We wish to express our thanks to Dr F. Bouquerel (Rhodia Technical Fibres) for helpful discussion and technical assistance and G. Pham (student at Ecole des Mines de Saint-Etienne) for his work on the correspondence between wear and fibre mechanical properties.

References

[1] Briscoe BJ, Evans PD, Pelillo E, Sinha SK. Wear 1996;200:137–47.
[2] Briscoe BJ, Pelillo E, Sinha SK. Polym Engng Sci 1996;36:2996–3005.
[3] Rajesh JJ, Bijwe J, Tewari US. Wear 2002;252:769–76.
[4] Budinski KG. Wear 1997;203–204:302–9.
[5] Voss H, Magill JH, Friedrich K. J Appl Polym Sci 1987;33:1745–61.
[6] Penning JP, Van Ruiten J, Brouwer R, Gabriëlse W. Polymer 2003;44:5869–76.
[7] Prevorsek DC, Harget PJ, Sharma RK, Reimschuessel AC. J Macromol Sci–Phys 1973;B8(1–2):127–56.
[8] Roselman IC, Tabor D. J Phys D: Appl Phys 1977;10:1181–95.
[9] Hernandez RJ, Gavara R. J Polym Sci, Part B: Polym Phys 1994;32:2367–74.
[10] Stuart B, Briscoe BJ. Polym Int 1995;38:95–9.
[11] Rubenstein C. J Appl Phys 1961;32:1445.
[12] Murthy NS, Bray RG, Correale ST, Moore RAF. Polymer 1995;36:3863–73.
[13] Cayer-Barrioz J, Mazuyer D, Kapsa Ph, Chateauminois A, Bouquerel F. Wear 2003;255:751–7.
[14] Drozdov A. Polym Engng Sci 1996;36:1907–19.
[15] Prevorsek DC, Kwon YD, Sharma RK. J Mater Sci 1977;12:2310–28.
[16] Plummer CJG, Goldberg A, Ghanem A. Polymer 2001;42:9551–64.
[17] Gensler R, Plummer CJG, Grein C, Kausch HH. Polymer 2000;41:3809–19.